Evaluation of Seismic Design Parameters for Metal Buildings with Heavy Wall and Heavy Roof in High Seismic Zones

Mohammad T. Nikoukalam.[1], Shahabeddin Torabian[2], Benjamin W. Schafer[3]

Abstract

The objective of this paper is to explore the seismic performance of metal building systems when they are designed as steel ordinary moment frames (OMFs), but have wall and roof dead loads that exceed prescriptive limits in the United States loads standard (ASCE 7). A set of archetype frames — spanning both clear span and modular metal building system geometries — was developed in collaboration with industry and subjected to a FEMA P-695-based seismic assessment. At the core of the assessment is an advanced shell finite element model of the metal building systems, exercised through a nonlinear hysteretic protocol to accurately capture the response of the system. The shell finite element models inform the calibration of nonlinear single-degree-of-freedom models used in incremental dynamic analyses under the FEMA P-695 ground motion suite. The results show that heavier roof and wall loads can reduce system ductility and collapse margins in certain configurations. However, all archetypes that satisfy a set of simple frame member proportioning criteria, achieve acceptable performance under the evaluated seismic demands. These findings support the extension of OMF-based designs to heavier wall and roof loads if the additional proportioning requirements are included.

Keywords

Metal buildings, seismic performance, non-linear, incremental dynamic analysis, fragility

1. Introduction

Steel ordinary moment frames (OMFs) are generally considered less ductile than special moment frames, and their use is typically restricted in high seismic design categories (SDC) D, E, and F per ASCE 7-16 (ASCE, 2016), which was used for design in this study. However, historical seismic performance of single-story OMFs — particularly in metal building systems with limited height, mass, and number of stories — has shown that these systems can perform adequately in strong ground motions. Following the 1994 Northridge earthquake, observations of metal building performance contributed to the development of ASCE 7 provisions that permitted OMFs in certain single-story structures. For instance, ASCE 7-98 (ASCE, 1998) and ASCE 7-02 (ASCE, 2002) allowed OMFs up to 60 ft [18.3 m] in height with roof dead loads below 15 psf [718 Pa],

[1] Mohammad T. Nikoukalam, PhD, PE, Consulting Engineer, Simpson Gumpertz & Heger Inc., Washington DC, United States, Email: mtnikoukalam@sgh.com

[2] Shahabeddin Torabian, PhD, PE, SE, Senior Project Manager, Simpson Gumpertz & Heger Inc., Washington DC, United States, Associate Scientist, Department of Civil and Systems Engineering, Johns Hopkins University, Baltimore, MD, United States, Email: storabian@sgh.com (Corresponding)

[3] Benjamin W. Schafer, PhD, PE, Consulting Principal, Simpson Gumpertz & Heger Inc., Washington DC, United States, Willard and Lillian Hackerman Professor, Department of Civil and Systems Engineering, Johns Hopkins University, Baltimore, MD, United States, Email: schafer@jhu.edu

specifically acknowledging bolted end-plate moment connections common in metal buildings. These provisions have since evolved and are currently found in ASCE 7-16 and ASCE 7-22 (ASCE, 2022) Sections 12.2.5.6.1 and 12.2.5.6.2.

With the introduction of the FEMA P-695 methodology (ATC, 2009), the Metal Building Manufacturers Association (MBMA) initiated a series of studies to evaluate whether OMFs used in metal buildings meet seismic performance expectations under current and extended design conditions. An initial peer-reviewed effort applied FEMA P-695 to index archetypes representing conventional clear-span buildings, including some with heavier wall systems such as archetype A1 and A2 (Moen et al., 2019) This study also used full-scale shake table testing of a specimen with precast concrete panels to validate modeling protocolsconfirming that such systems satisfy collapse performance objectives when designed with a response modification factor R = 3.5 (Meimand et al., 2018; Moen et al., 2019). Although these heavy wall configurations were shown to meet FEMA P-695 collapse safety criteria, their performance was assessed within a narrow design space (clear span and light roof), without establishing general geometric or structural limits for broader code application. That work laid the foundation for a validated high-fidelity modeling framework — supported by experimental research including shake table and component testing (Smith et al., 2013; Uang et al., 2011) — that has since been extended to modular building configurations in a follow-up study by Nikoukalam et al. (2025).

Building on those prior evaluations, the present study uses the framework of Moen et al. (2019) to investigate the seismic performance of both clear span and modular metal buildings with increased roof and wall dead loads (e.g. precast concrete walls) and heights beyond ASCE 7 limits, per the FEMA P-695 methodology. A suite of archetype buildings representing both clear span and modular configurations was developed in collaboration with industry partners to reflect practical design scenarios beyond the limits evaluated in previous studies, and beyond those specified by ASCE 7. Each archetype was analyzed using modal analysis, nonlinear static and cyclic analysis, and dynamic procedures to assess key performance metrics including system overstrength, ductility, and collapse margin. The study quantifies the impact of increased seismic mass on system behavior and establishes additional proportioning criteria that ensure acceptable performance under the FEMA P-695 framework.

2. Design of Metal Building Archetypes

A critical step in the seismic performance evaluation under FEMA P-695 is the development of representative building archetypes. In prior work, archetypes were established for clear span and modular metal buildings under typical wall and roof load conditions (Moen et al., 2019; Nikoukalam et al., 2025). In the current study, a total of eight archetypes were developed, consisting of four modular buildings evaluated with increased wall loads (designated as M-HW: Modular – Heavy Wall) and four clear span buildings evaluated with increased roof loads (designated as C-HR: Clear Span – Heavy Roof). Table 1 summarizes the building geometries and design loads.

All M-HW archetypes have a building height of 45 ft [13.7 m] (which is more than the 35ft [10.7 m] limit in ASCE 7) and consist of two spans of either 50 ft or 100 ft [15.2 m or 30.4 m], with a longitudinal bay spacing of 25 ft [7.6 m]. Two roof dead load levels are considered: 20 psf and 30 psf [958 Pa and 1440 Pa], while the wall panel self-weight is consistently taken as 116 psf [5550 Pa], representing a 9.25 in. [235 mm] thick precast concrete wall panel.

The C-HR archetypes have single span frames with heights of either 25 ft or 45 ft [7.6 m or

13.7 m] and spans of 50 ft or 100 ft [15.2 m or 30.4 m]. A roof dead load of 30 psf [1440 Pa] is applied to all clear span buildings, while wall panel self-weight is approximately 2 psf [96 Pa], consistent with typical light cladding systems. All clear span buildings share the same 25 ft [7.6 m] longitudinal bay width. These archetypes isolate the influence of increased roof load on seismic behavior while keeping other parameters in line with previous studies.

The archetypes were designed and detailed by engineers from Metal Building Manufacturers Association (MBMA) member companies using their own in-house design, optimization, and detailing software, based on the geometric and loading parameters defined in Tables 1 and 2. All buildings were designed as Risk Category II structures subjected to Design Earthquake (DE) ground motions per ASCE 7-16. Note, the bracing provisions of AISC 360 Appendix 6 (AISC, 2016) were enforced in all designs, as they were previously found to be critical in ensuring acceptable ductility (Nikoukalam et al., 2025).

To ensure that frame designs were governed by seismic loads, snow load combinations were not considered. Secondary structural elements such as purlins, girts, roof decks, diaphragms, and lateral braces were designed for wind loads representative of the average component and cladding pressures in the United States, corresponding to a wind speed of 110 mph [177 kph]. However, seismic loads governed the design of the primary frames. Seismic parameters such as spectral response accelerations and site class follow FEMA P-695 recommendations for a typical high seismic region, see Tables 1 and 2 for the full design narrative details.

Table 1: Metal building archetypes dimensions and design loads

Archetype	Roof Dead Load		Wall Panel Self-weight		H	N × Span	Bay	V_r
		psf [Pa]		psf [Pa]	ft [m]	N × ft [m]	ft [m]	kip [kN]
M-HW-1	Light	20 [958]	Heavy[b]	116 [5554]	45 [13.7]	2 × 50 [15.2]	25 [7.6]	127.8 [568]
M-HW-2	Light	20 [958]	Heavy	116 [5554]	45 [13.7]	2 × 100 [30.4]	25 [7.6]	142.7 [635]
M-HW-3	Heavy[a]	30 [1436]	Heavy	116 [5554]	45 [13.7]	2 × 50 [15.2]	25 [7.6]	123.4 [549]
M-HW-4	Heavy	30 [1436]	Heavy	116 [5554]	45 [13.7]	2 × 100 [30.4]	25 [7.6]	171.8 [764]
C-HR-1	Heavy	30 [1436]	Light	~ 2 [96]	25 [7.6]	1 × 50 [15.2]	25 [7.6]	23.9 [106]
C-HR-2	Heavy	30 [1436]	Light	~ 2 [96]	45 [13.7]	1 × 50 [15.2]	25 [7.6]	23.6 [105]
C-HR-3	Heavy	30 [1436]	Light	~ 2 [96]	25 [7.6]	1 × 100 [30.4]	25 [7.6]	43.2 [192]
C-HR-4	Heavy	30 [1436]	Light	~ 2 [96]	45 [13.7]	1 × 100 [30.4]	25 [7.6]	43.6 [194]

a. Heavy roof dead load is defined as 30 psf [1440 Pa] which is in excess of ASCE 7-16 limit
b. Heavy wall self-wight is defined as 116 psf [5550 Pa] and is based on a typical precast concrete wall panel

100 **Table 2. Archetype design assumptions**

Summary of Demand Side (ASCE 7) Design Assumptions	
Building Risk Category	II
Roof slope	1:12
Roof dead load (psf [Pa])	2.2 [105.3]
Self-weight (psf [Pa])	2.5 [119.7]
Collateral dead load (psf [Pa])	15 [718] for light roof designs 23 [1101] for heavy roof designs
Roof live (reducible) (psf [Pa])	20 [957.6]
Snow load (psf [Pa])	0 [0]
Rain load (psf [Pa])	0 [0]
Wind speed (mph [kph])	110 [177]
Wind exposure category	B
Seismic Importance Factor	1.0
Seismic Design Category	D
Site Class	D
F_a, F_v	1, 1.7
S_s (g), S_1 (g)	1.5, 0.6
S_{DS}, S_{D1}	1, 0.68
R, Ω_o, C_d	3.5, 2.5, 3
Redundancy Factor (ρ)	1.3
Design Method	Allowable Stress Design
Seismic load	Equivalent Lateral Force Procedure
Drift Limit	Δ_a = H/40
Summary of Capacity Side (AISC 360) Design Assumptions	
Metal Building Frame	OMF Ordinary Moment Frame
Seismic detailing specifications	Three-plate members, pinned base, no restriction on member compactness, no restriction on member splice locations, no restrictions on taper, pinch point, belly points, no special design of the panel zone
AISC 341 Seismic Provisions: Overstrength conditions	AISC Design Guide 16 Connection Type, Design knee connection with R=1.0 Use Ω_o forces only for column and base plate axial load including anchor rods and welding.
Material	Specified F_y = 55 ksi [379 MPa], F_u = 70 ksi [482 MPa]
Welding	AWS D1.8 provisions, no protected zones
Anchor Rods	ASTM F1554 Grade 36

101

102 3. Numerical Modelling

103 The numerical modeling framework used in this study follows the high-fidelity finite element
104 approach previously developed for metal building seismic performance evaluation (Meimand et
105 al., 2018; Moen et al., 2019) and extended in later modular frame studies by Nikoukalam et al.,
106 (2025). The modeling approach was validated against subassembly tests conducted per AISC 341-
107 10 (AISC, 2010; Smith et al., 2013) and full-scale shake table tests at University of California San
108 Diego (UCSD) (Smith et al., 2013; Uang et al., 2011).

109 All finite element simulations were conducted in ABAQUS (Simulia, 2014), with automated
110 input file generation via MATLAB scripts (MathWorks, 2018). Primary frame members—
111 including built-up, tapered columns and rafters — were modeled using S4R shell elements (Figure
112 1), following mesh density guidelines from Schafer, Li, and Moen (Schafer et al., 2010), with a
113 minimum of four nodes per local buckling half-wavelength. Local and global imperfections were

included: a web distortion pattern with $\delta = h/250$ and a global sweep of $L/1000$ (Smith, 2013). Residual stresses were modeled using thermal self-equilibrating distributions based on Prawel, Morrell, and Lee (Prawel et al., 1974) and Kim (Kim, 2010).

Steel material behavior was defined using an isotropic plasticity model with a yield stress of 55 ksi [379 MPa] and ultimate stress of 70 ksi [482 MPa]. Secondary elements with open cold-formed steel sections such as purlins, girts, and roof and wall panels were modeled using shell elements, rod braces were modeled using beam elements, and fasteners represented using multi-point constraints.

In modular buildings (M-HW archetypes), the wall system consisted of concrete panels rather than steel wall panels. These panels were modeled using shell elements and connected to the structural frame via multi-point constraints. Additionally, spandrel beams were used in place of girts to support the wall panels. These beams were modeled using shell elements, consistent with the modeling of primary frame components. In contrast, C-HR buildings used conventional steel wall panels, as in the previous study, and girts were included as part of the secondary framing system. Further modeling assumptions, boundary conditions, and connection modeling details are provided in Nikoukalam et al. (Nikoukalam et al., 2025).

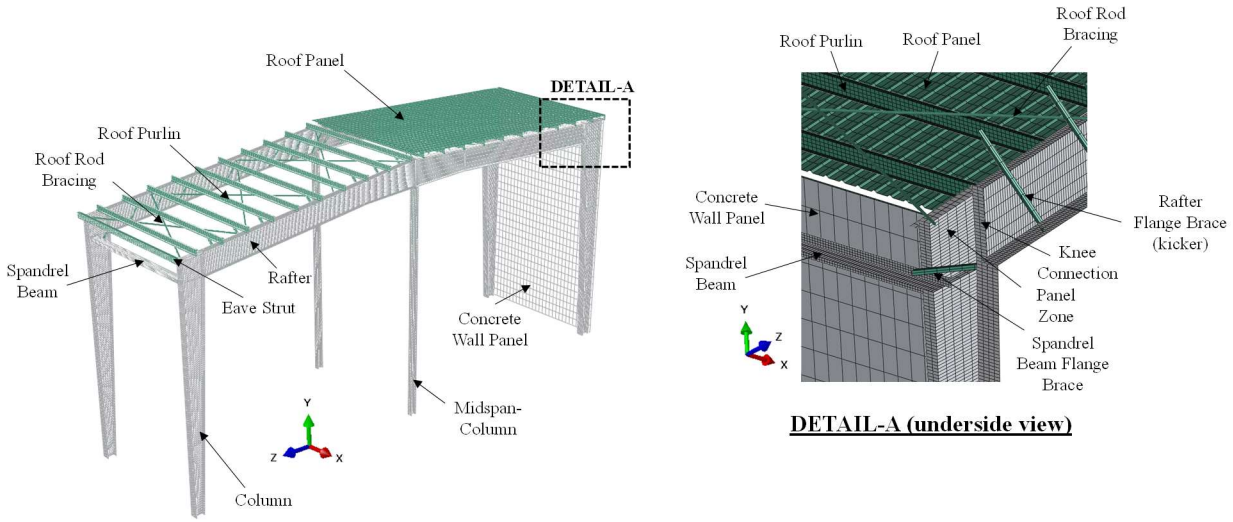

Figure 1. Annotated example metal building system high fidelity finite element model

4. Analysis and Evaluation of Archetype Buildings

4.1. Pushover Analysis

Prior to conducting nonlinear cyclic or dynamic analyses, nonlinear static pushover analyses were performed for all archetypes. These analyses were used to evaluate the system overstrength (Ω_0), ductility (μ), and period-based ductility (μ_T) parameters in accordance with FEMA P-695. The pushover results also serve to verify the accuracy of the model, identify the governing failure mechanisms, and assist in defining drift-based collapse limits (see Section 4.4). The high-fidelity models are fully nonlinear with respect to both material and geometry, including large deformation effects (P-Δ and P-δ).

Figure 2 presents the base shear–roof displacement response for all modular buildings (M-HW archetypes) and Figure 4 shows their corresponding deformed shapes and stress contours. All M-HW buildings demonstrated sufficient ductility for acceptable seismic performance. The initial limit state in each case involved a combination of rafter yielding, local buckling, and lateral-torsional buckling (LTB).

Figure 3 provides the static pushover response for the C-HR buildings. the pushover responses for the clear span (C-HR) archetypes. The short buildings, C-HR-1 and C-HR-3, showed stable post-peak behavior and adequate ductility. Their first limit states involved rafter yielding, local buckling, and LTB (Figure 5).

In contrast, the tall clear span archetypes, C-HR-2 and C-HR-4, experienced more than 20% strength degradation at peak base shear, indicating insufficient ductility. The observed post-peak response for C-HR-2 and C-HR-4 are provided in Figure 6(a) and (c) respectively. Although both had peak strengths well above their design base shear, their post-peak response was dominated by rafter lateral-distortional buckling (LDB)—a mode characterized by top flange translation coupled with web bending (Figure 7(b)). This failure mechanism is not explicitly addressed in current AISC design specifications but becomes significant for certain cross-section geometries and unbraced lengths.

Geometric data analysis of the modeled frames (Figure 8), focusing on the dimensions at the first brace away from the knee in the rafter, revealed common features among the underperforming clear span frames:

- h/b_f ratios greater than 6
- A_w/A_f ratios greater than 2.5

Where h is the clear distance of the web, b_f is the total flange width, A_w is the area of the web and A_f is the area of the flange. That is, in the poor performing frames the rafter is overly tall and narrow with the web carrying a large amount of the demand. These proportioning characteristics are the same required to develop stable shear post-buckling through tension field action (TFA) as specified in AISC 360-16 Section G2.2 (AISC, 2016). Based on this observation, C-HR-2 and C-HR-4 were redesigned by MBMA engineers to meet the AISC 360 TFA proportioning limits. The updated archetypes, labeled C-HR-2R and C-HR-4R, were reassessed using the same pushover protocol. Their responses are shown in Figure 3 and their deformed shapes in Figure 6(b) and (d), respectively. The redesigns led to improved ductility and shifted the governing limit state from rafter LDB to panel zone yielding and local buckling, resulting in overall acceptable performance.

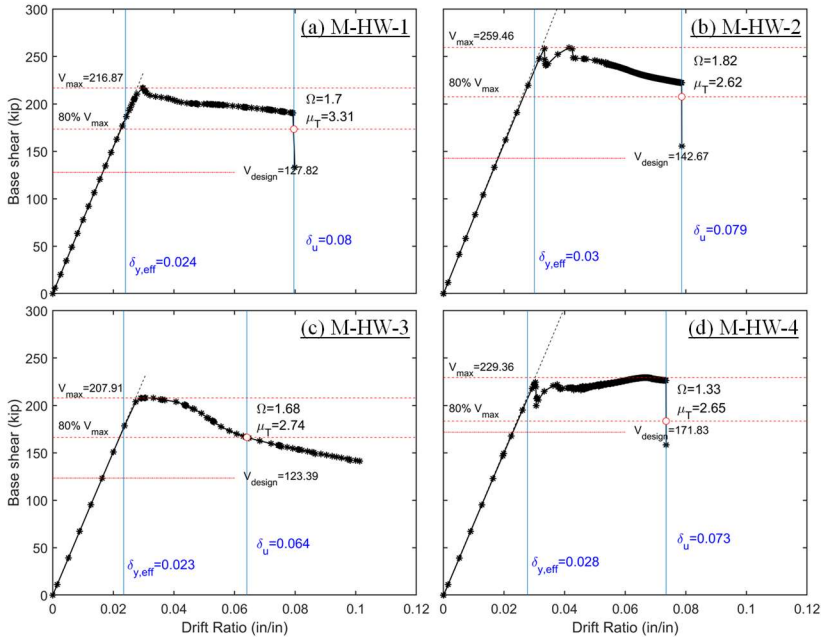

175
176 **Figure 2. Static pushover curve of modular heavy wall archetypes [1 kip = 4.448 kN]**

177

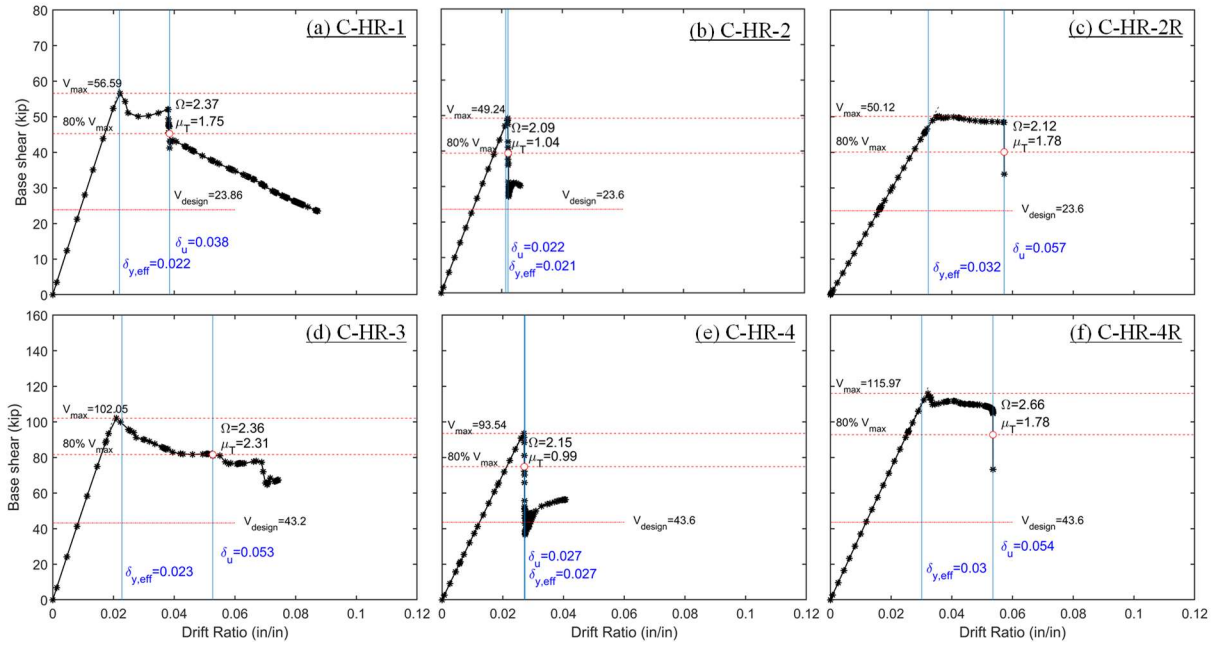

178
179 **Figure 3. Static pushover curve of clear-span heavy roof archetypes [1 kip = 4.448 kN]**

180 The nonlinear static pushover analysis provides a clear assessment of the governing limit states
181 in each archetype. The sequence of failure mechanisms observed across the full drift range is
182 summarized in Table 3.

Table 3. Sequence of observed behavior in each archetype

Archetype	Observed Behaviour					
	Drift (%)	**First significant Behavior**	**Drift (%)**	**Post-peak Behavior**	**Drift (%)**	**Large-drift Behavior**
M-HW-1	3.8	Rafter Y and LB	5.0	Rafter Y and LB PZ Y	-	-
M-HW-2	3.4	Rafter Y and LB	4.3	Rafter Y, LB, and LTB PZ Y	-	-
M-HW-3	3.7	Rafter Y, LB, and LTB	4.4	Rafter Y, LB, and LTB Purlin LTB	5.3	Rafter Y, LB, and LTB Purlin LTB PZ Y
M-HW-4	3.8	Rafter Y, LB, and LTB	4.3	Rafter Y, LB, and LTB Purlin LTB	5.7	Rafter Y, LB, and LTB Purlin LTB PZ Y
C-HR-1	2.8	Rafter Y, LB, and LTB	3.9	Rafter Y, LB, and LTB Column LB		
C-HR-2R	3.6	PZ Y	4.2	PZ Y and LB Column Y and LB		
C-HR-3	2.4	Rafter Y, LB, and LTB	5.4	Rafter Y, LB, and LTB Purlin LTB		
C-HR-4R	3.3	PZ Y	4.3	PZ Y and LB Rafter Y, LB, and LTB		
Designs prior to redesign per AISC 360, Section G2.2						
C-HR-2	2.2	Rafter LDB and LTB Purlin LTB				
C-HR-4	2.7	Rafter LDB and LTB				

Note: Y: Yielding, LB: Local Buckling, LTB: Lateral-Torsional Buckling, LDB: Lateral Distortional Buckling, PZ: Panel Zone

Major observations from the nonlinear static response include:

- In the modular heavy wall (M-HW) buildings, the first significant behavior consistently involved rafter yielding and local buckling near the haunch region. For M-HW-1 and M-HW-2, no significant strength degradation occurred beyond initial limit states, and panel zone yielding appeared only at higher drift levels. For M-HW-3 and M-HW-4, lateral-torsional buckling (LTB) in the rafter and purlin LTB appeared in the post-peak and large-drift stages, but the overall behavior remained stable.
- In the clear span heavy roof (C-HR) archetypes, short buildings (C-HR-1 and C-HR-3) exhibited limit states involving rafter yielding, local buckling, and LTB. At higher drift levels, C-HR-1 showed minor column local buckling, and C-HR-3 developed purlin LTB, but neither affected overall system performance. These frames demonstrated sufficient strength and ductility for seismic design compliance.
- The original tall clear span buildings, C-HR-2 and C-HR-4, exhibited lateral-distortional buckling (LDB) in the rafters at low drift levels, followed by purlin LTB. These failure modes resulted in a brittle post-peak response and inadequate ductility. Their behavior reinforced the importance of section proportioning for tall, clear span frames and led to the identification of two key geometric limits related to h/b_f and A_w/A_f ratios (see Section 4.1 discussion above).
- The redesigned tall clear span archetypes, C-HR-2R and C-HR-4R, implemented the AISC 360 G2.2-based proportioning limits. As a result, the failure modes transitioned

from rafter LDB to more ductile mechanisms such as panel zone yielding, local buckling, and in some cases minor rafter LTB. These redesigned configurations achieved stable post-peak behavior, validating the proposed proportioning criteria.

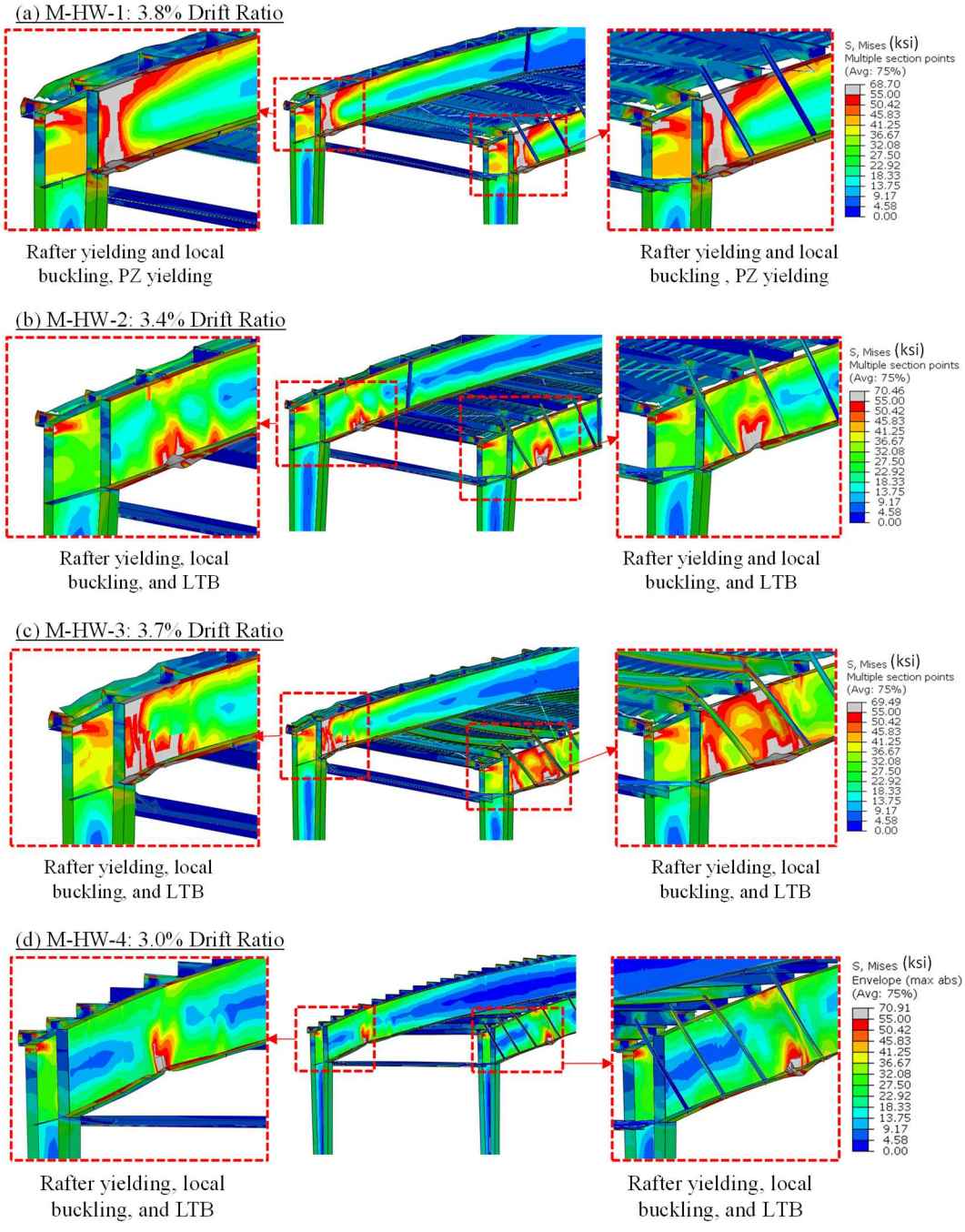

213 **Figure 4. First failure mode in modular heavy wall: (a) M-HW-1, (b) M-HW-2, (c) M-HW-3, (d) M-**
214 **HW-4 [1 ksi = 6.89 MPa]**

215

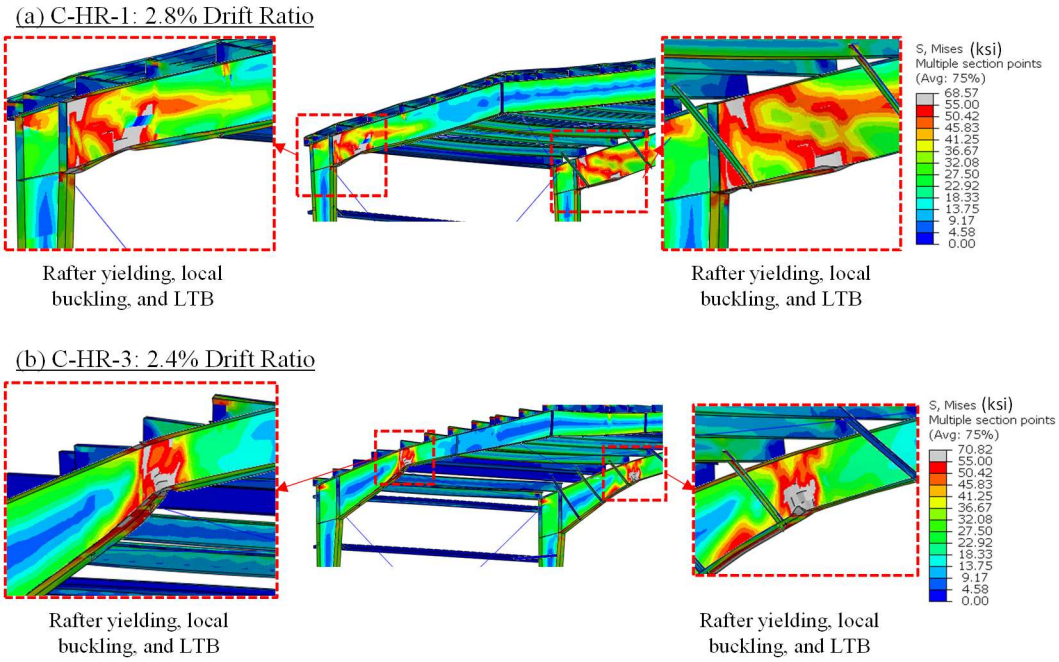

216
217 **Figure 5. First failure mode in short clear-span heavy roof buildings (h = 25 ft [7.6 m]): (a) C-HR-1,**
218 **(b) C-HR-3 [1 ksi = 6.89 MPa]**

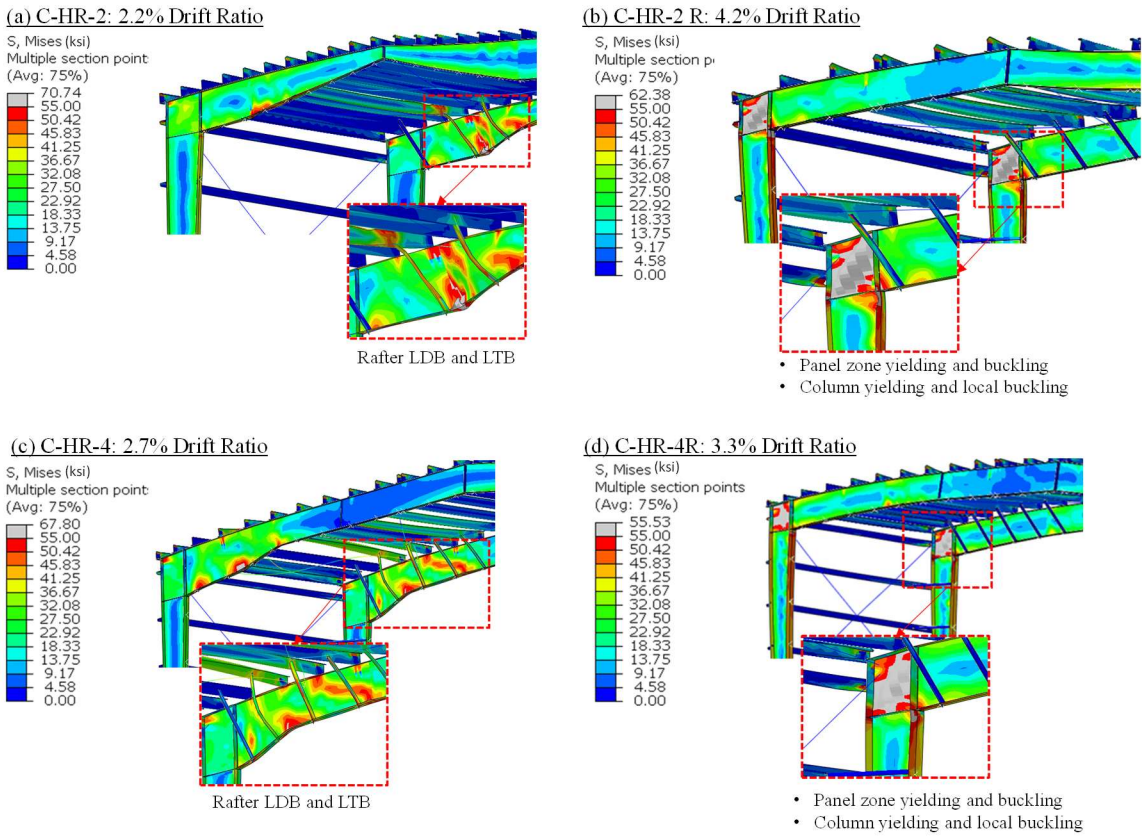

Figure 6. First failure mode in tall clear-span heavy roof buildings (h = 45 ft [13.7 m]): (a) C-HR-2, (b) C-HR-2R, (b) C-HR-4, (b) C-HR-4R [1 ksi = 6.89 MPa]

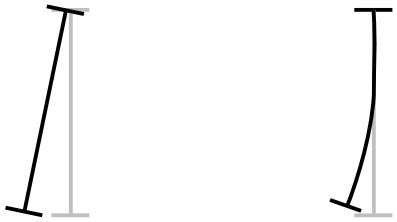

(a) Lateral Torsional Buckling (LTB)

(b) Lateral Distortional Buckling (LDB)

Figure 7. Lateral Torsional Buckling (LTB) vs Lateral Distortional Buckling (LDB) of I-shape sections

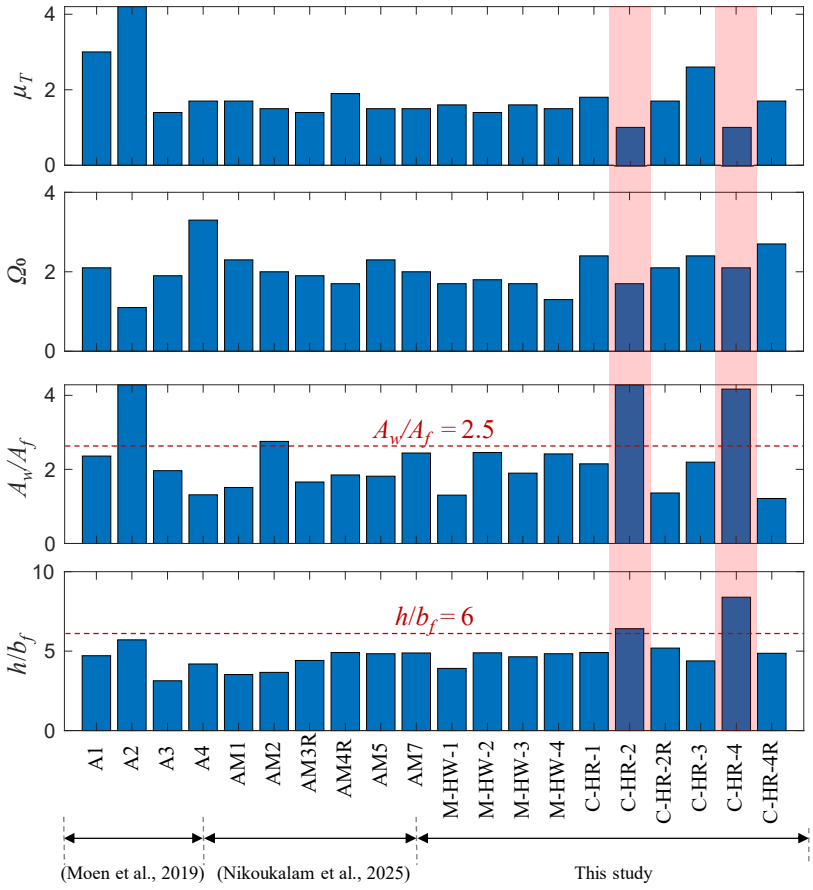

Figure 8. Geometric data analysis of the modeled archetype buildings studied during 2018-2025, focusing on the dimensions at the first brace away from the knee in the rafter

The resulting system overstrength (Ω_0), ductility (μ), and period-based ductility (μ_T) for each archetype are summarized in Table 4. These parameters were computed from the nonlinear static pushover responses in accordance with FEMA P-695. The definitions and calculation methodology follow the procedures outlined in FEMA P-695 and previously documented by Nikoukalam et al. (2025). Effective yield displacement for μ_T calculations incorporates the larger of the ASCE 7-16 design period and the fundamental period obtained from eigenvalue analysis (see Section 4.2).

According to Table 4, the calculated overstrength factors are in the range of 1.3 to 2.7. According to the FEMA P-695 procedures, the system overstrength, Ω_o, is calculated as the maximum of the average from the different performance groups, but not to exceed a maximum value of Ω_o=3.0. Accordingly, from the archetype analysis summarized in Table 4, the design value would be set to Ω_o=2.0, governed by the average value of the performance group.

Table 4. Summary of system overstrength (Ω_o) and period-based ductility (μ_T) factors for each archetype

	Archetype	Overstrength	Ductility	Period-Based Ductility
		Ω_o	μ^b	$\mu_T{}^b$
Modular Heavy Wall	M-HW-1	1.7	>1.61	>1.87
	M-HW-2	1.82	>1.39	>1.50
	M-HW-3	1.68	1.61	1.88
	M-HW-4	1.31	>1.52	>1.66
	Average	1.63	>1.53	>1.73
Clear-span Heavy Roof	C-HR-1	2.4	1.8	1.75
	C-HR-2R	2.1	>1.70	>1.78
	C-HR-3	2.4	2.60	2.31
	C-HR-4R	2.7	>1.70	>1.78
	Average	2.4	>1.95	>1.91
	Designs prior to redesign per AISC 360, Section G2.2			
	C-HR-2	1.7	1.00[a]	1.00[a]
	C-HR-4	2.1	1.00[a]	1.00[a]

[a] premature failure
[b] at 4.5% drift ratio

4.2. Frequency (Modal) Analysis

The natural periods and mass participation ratios for all archetypes are summarized in Table 5. The results are based on eigenvalue analysis of the high-fidelity shell models, with first-mode mass participation ranging from 0.87 to 0.99. As expected, modular buildings (M-HW archetypes) exhibit longer periods than clear span buildings due to their increased flexibility and gravity-only interior columns.

The modular heavy wall (M-HW) archetypes have fundamental periods between 1.55 and 2.00 seconds. These relatively long periods reflect the increased height (45 ft [13.7 m]), heavier wall systems, and longer spans supported by gravity-only interior columns. In contrast, the clear span heavy roof (C-HR) buildings exhibit shorter periods, ranging from 0.98 to 1.72 seconds, depending on height and span. As expected, taller clear span frames show longer periods than their shorter counterparts.

Across all archetypes, the empirical period estimates from ASCE 7-16 (Eq. 12.8-7) significantly underpredict the actual periods observed in the high-fidelity models, with ratios of T_1/T_{ASCE7} ranging from approximately 2.4 to 3.2. In contrast, the periods used in industry design—based on beam element approximations—exhibit closer agreement with the shell model results, generally falling within 10–15%.

Additional details regarding the modal analysis procedures and underlying modeling assumptions can be found in Nikoukalam et al. (2025).

Table 5. Summary of the modal analysis results of the high-fidelity models and period evaluation of the archetype buildings per ASCE 7-16 method

Archetype	mass participation ratio	T_1 (s)	T_{ASCE7} (s)	T_{Design} (s)	$\frac{T_1}{T_{ASCE7}}$	$\frac{T_1}{T_{Design}}$
M-HW-1	0.91	1.55	0.61	NA	2.54	NA
M-HW-2	0.88	1.79	0.63	1.80	2.84	0.99
M-HW-3	0.91	1.64	0.61	1.69	2.69	0.97
M-HW-4	0.87	2.00	0.63	1.81	3.17	1.11
C-HR-1	0.99	0.99	0.38	NA	2.61	NA
C-HR-2	0.97	1.42	0.60	1.46	2.37	0.97
C-HR-2R	0.97	1.72	0.60	1.96	2.87	0.88
C-HR-3	0.88	0.98	0.39	0.91	2.51	1.07
C-HR-4	0.97	1.62	0.61	1.49	2.66	1.09
C-HR-4R	0.97	1.54	0.61	1.45	2.52	1.06

T_1: first period of high fidelity shell finite element model
T_{ASCE7}: estimate period based on ASCE 7-16, Eq. 12.8-7
T_{Design}: period estimate by metal building designer based on beam element approximation

4.3. Cyclic Analysis

Quasi-static cyclic simulations were conducted on the high-fidelity models of each archetype to evaluate strength and stiffness degradation under repeated lateral loading. The simulations follow the cyclic displacement protocol specified in AISC 341, applied horizontally at the rafter-column knee level. The resulting hysteretic behavior is expressed in terms of base shear versus story drift ratio and is presented in Figure 9 for the modular heavy wall (M-HW) buildings and Figure 10 for the clear span heavy roof (C-HR) buildings.

The cyclic responses generally trace the same envelope as the monotonic backbone curves, but with some additional degradation in strength and stiffness across cycles. This degradation is modest in most cases, and the post-peak behavior remains stable in all archetypes.

The cyclic response results are used to calibrate nonlinear single-degree-of-freedom (SDOF) models for each archetype. These calibrated SDOF representations form the basis for the incremental dynamic analyses (IDA) discussed in the following section.

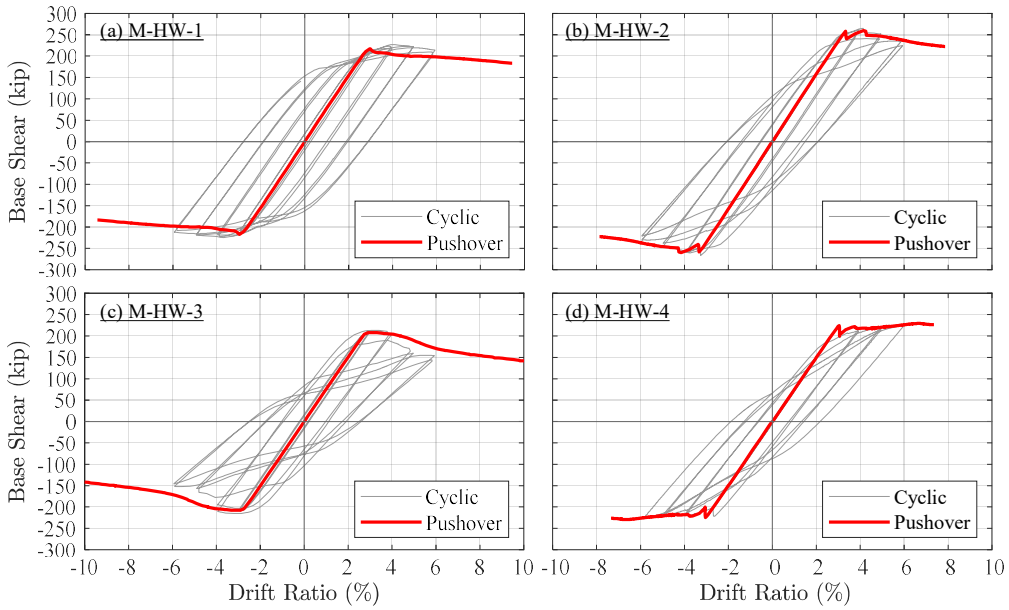

Figure 9. Quasi-cyclic and pushover response of modular heavy wall buildings [1 kip = 4.448 kN]

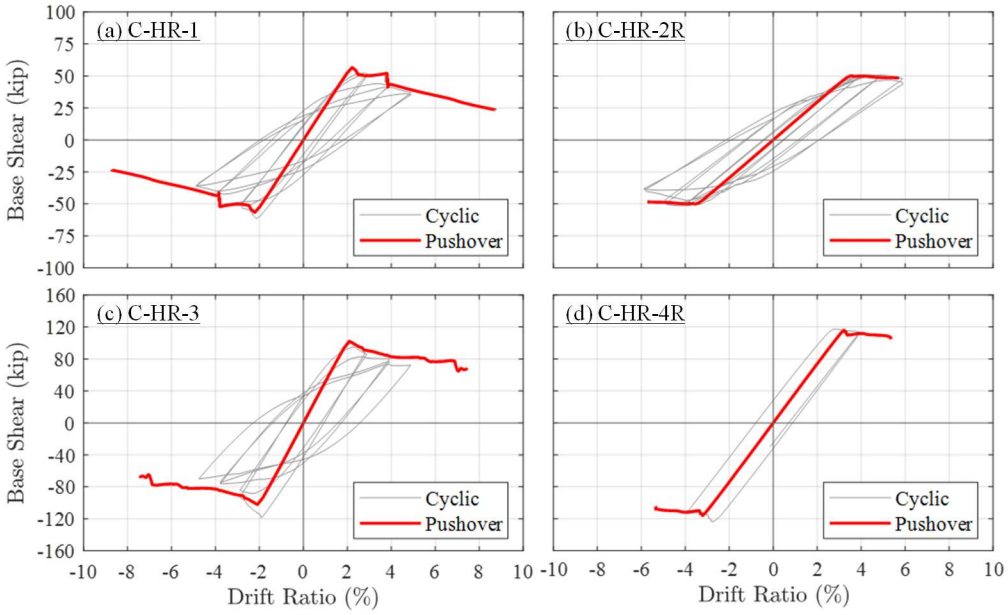

Figure 10. Quasi-cyclic and pushover response of clear-span heavy roof buildings [1 kip = 4.448 kN]

4.4. Incremental Dynamic Analysis (IDA)

Incremental dynamic analyses (IDA) were conducted for each archetype using the FEMA P-695 methodology to assess collapse performance and determine the acceptability of the seismic response modification factors used in design. Each archetype was represented by a calibrated nonlinear single-degree-of-freedom (SDOF) model (Figure 11), which was subjected to the far-field ground motion set recommended in FEMA P-695 Appendix A, comprising 22 pairs (44 total) of horizontal records.

As in previous work (Nikoukalam et al., 2025), the SDOF system was calibrated to replicate both the cyclic backbone and dynamic properties of the corresponding high-fidelity finite element model. The simplified model is shown schematically in Figure 11, where the structural system is represented by a lumped mass, a nonlinear spring, and linear viscous damping. The hysteretic behavior of the spring is modeled using the Pinching 04 material in OpenSees (McKenna et al., 2004), which captures strength and stiffness degradation as well as pinching under reversed cyclic loading. Four key response points define the monotonic envelope of the hysteretic model, and additional parameters control unloading behavior and degradation (see Figure 12). These parameters were tuned to minimize the cycle-by-cycle error between the SDOF and high-fidelity cyclic responses and are provided in Appendix, Table A.

The equivalent seismic mass was taken as the design seismic weight of the building, and the initial stiffness of the SDOF model was computed to match the fundamental period obtained from modal analysis. This approach follows the procedure detailed in FEMA P-695 Chapter 6. A damping ratio of 2% was applied for all analyses, representing elastic energy dissipation, while all inelastic mechanisms are accounted for within the hysteretic model.

In this study, a collapse drift limit of 4.5% was adopted for all archetypes. This limit is consistent with values used in earlier studies on metal buildings (Moen et al., 2019) and reflects

the drift range at which significant local damage—such as panel zone yielding, flange local buckling, or cyclic strain accumulation—can compromise the load-carrying capacity of the system. Unlike the more flexible modular archetypes from the previous phase (Nikoukalam et al., 2025), several buildings studied here begin exhibiting nonlinear response prior to 4.5% drift, making this limit both conservative and appropriate for defining collapse in the IDA framework. Further details on the modeling approach and calibration process can be found in Nikoukalam et al. (2025).

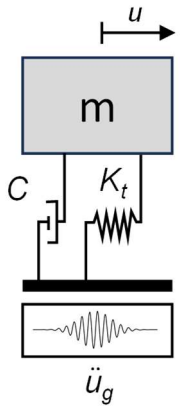

Figure 11. Metal building non-linear SDOF model definitions (Nikoukalam et al., 2025)

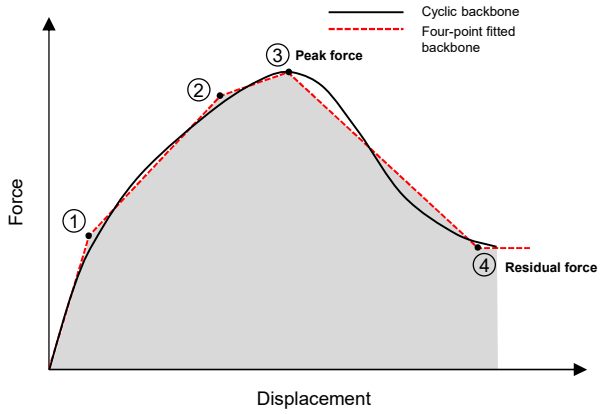

Figure 12. A four-point backbone fitted to the cyclic backbone is shown in the first quadrant (Nikoukalam et al., 2025)

The IDA results for the modular heavy wall (M-HW) and clear-span heavy roof (C-HR) archetypes are presented in Figure 13 and 14, respectively. Each figure shows the base shear versus drift IDA curves and the corresponding collapse fragility curves. For each archetype, the median collapse intensity, $\hat{S}_{CT}$, is determined from the IDA results, and the collapse margin ratio (*CMR*) is computed as $\hat{S}_{CT}$ / S_{MT}, where S_{MT} is the maximum considered earthquake (MCE) spectral acceleration at the fundamental period.

To account for the influence of spectral shape, a spectral shape factor (*SSF*) is applied to adjust the *CMR*, resulting in the adjusted collapse margin ratio (*ACMR* = *SSF* × *CMR*). The *SSF* is a function of the fundamental period and the period-based ductility μ_T, and is computed per FEMA P-695 guidelines. Final *ACMR* values for all archetypes are summarized in Table 6.

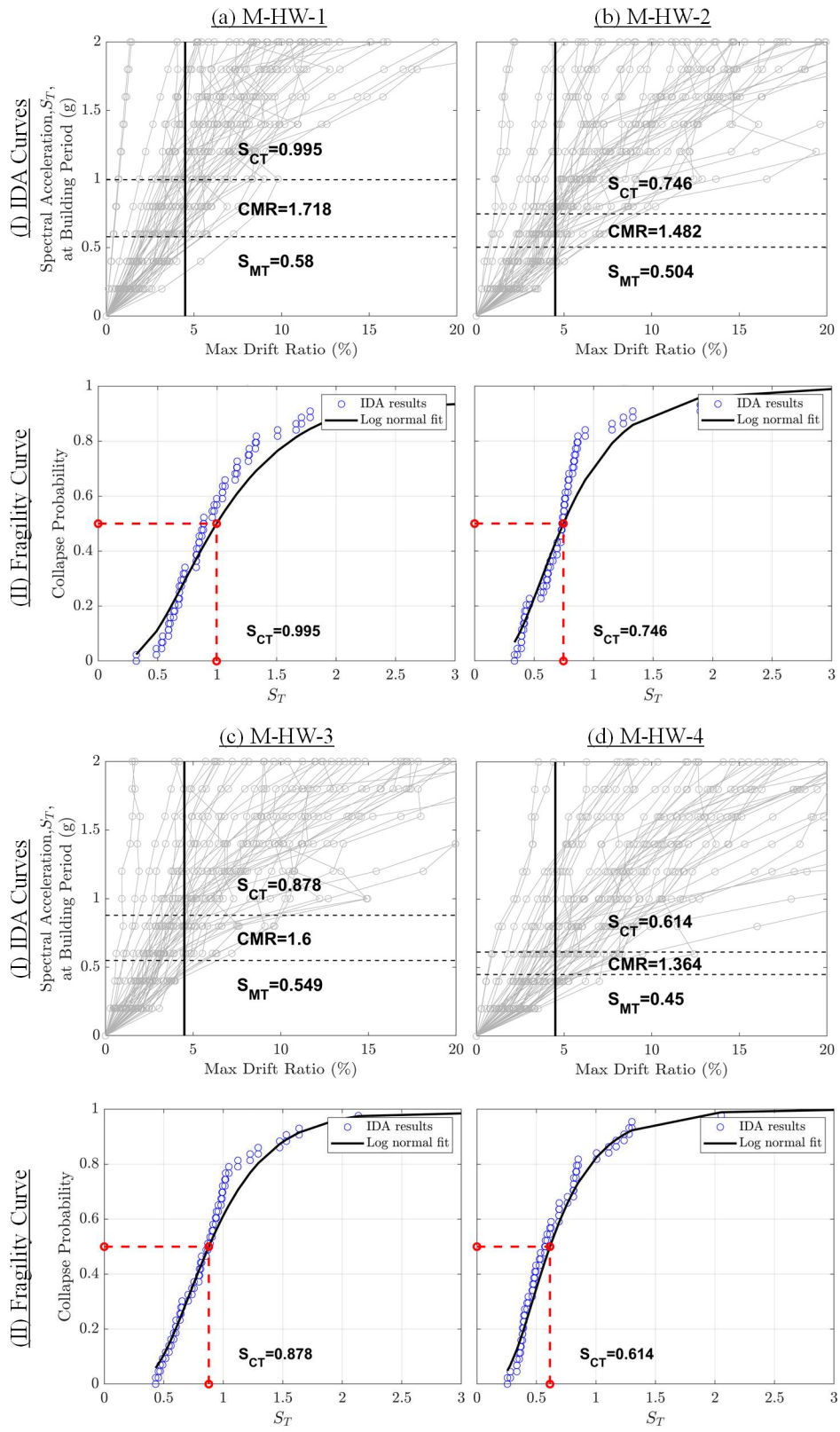

335
336 **Figure 13. IDA and fragility curves for heavy wall archetype buildings**

337

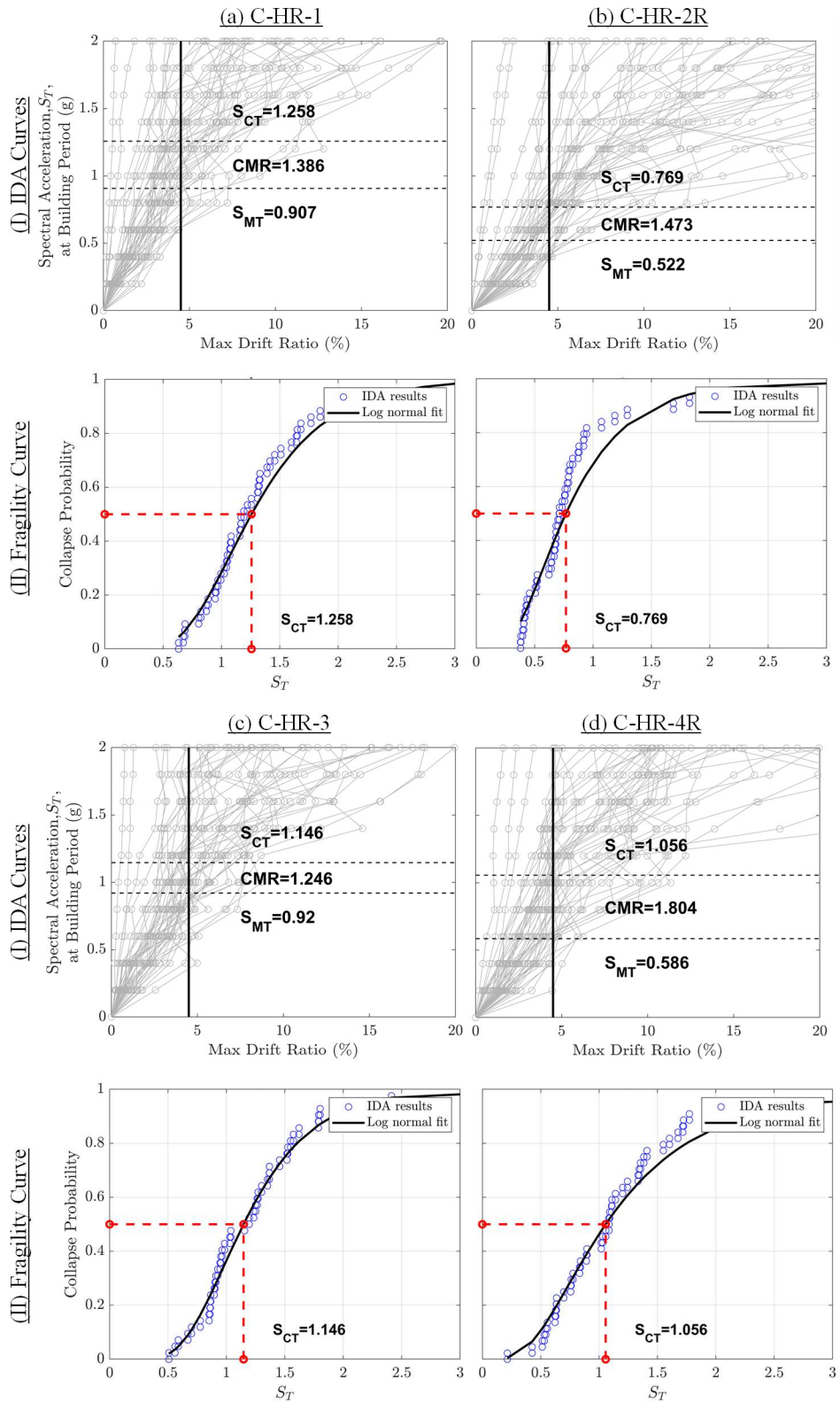

338

339 **Figure 14. IDA and fragility curves for clear span heavy roof archetype buildings**

4.5. Seismic Performance Assessment per FEMA P-695 Approach

In accordance with FEMA P-695, the seismic performance of each archetype is evaluated based on its adjusted collapse margin ratio (*ACMR*). Each archetype must exceed the individual acceptable collapse margin ratio ($ACMR_{20\%}$), and the performance group average must exceed the group threshold ($ACMR_{10\%}$). These limits correspond to collapse probabilities of 20% and 10%, respectively, under MCE-level ground motions.

The acceptable *ACMR* values are calculated assuming a lognormal distribution of collapse intensities, with a median equal to $\hat{S}_{CT}$, and a standard deviation of β_{TOT}, which represents the total uncertainty in the collapse behavior of the system calculated as:

$$\beta_{TOT} = \sqrt{\beta_{RTR}^2 + \beta_{DR}^2 + \beta_{TD}^2 + \beta_{MDL}^2} \quad (1)$$

Following FEMA P-695 guidance and prior work (Nikoukalam et al., under review), the component uncertainties were taken as:

- $\beta_{DR} = 0.20$, reflecting professionally engineered and peer-reviewed designs,
- $\beta_{TD} = 0.20$, based on availability of high-quality shake table and subassembly test data,
- $\beta_{MDL} = 0.10$, due to the validated high-fidelity and SDOF models, and
- $\beta_{RTR} = 0.1 + 0.1\mu_T \leq 0.4$, representing record-to-record variability.

Table 6 summarizes the key parameters for all archetypes, including overstrength (Ω_o), period-based ductility (μ_T), median collapse capacity ($\hat{S}_{CT}$), MCE spectral intensity (S_{MT}), collapse margin ratio (*CMR*), spectral shape factor (*SSF*), adjusted collapse margin ratio (*ACMR*), and the acceptance thresholds $ACMR_{10\%}$ and $ACMR_{20\%}$.

All archetypes in both performance groups—modular heavy wall (M-HW) and clear-span heavy roof (C-HR)—exceed the required collapse safety limits individually and on average. As a result, the use of seismic design parameters $R = 3.5$, $\Omega_o = 3$, and $C_d = 3$ is validated for these building types under the applied configurations.

Table 6. Summary of archetypes analyses results: collapse drift limit of 4.5% (R = 3.5, Ω_o = 3, C_d = 3)

Archetype	Ω_o	μ_T	S_{CT}	S_{MT}	CMR	SSF	$ACMR$	$ACMR_{10\%}$	$ACMR_{20\%}$	Check (Pass/Fail)
	(-)	(-)	(g)	(g)	(-)	(-)	(-)	(-)	(-)	
M-HW-1	1.7	1.87	1.00	0.58	1.72	1.21	2.09	1.70	1.42	Pass
M-HW-2	1.8	1.50	0.75	0.50	1.48	1.17	1.73	1.65	1.39	Pass
M-HW-3	1.7	1.88	0.88	0.55	1.60	1.22	1.94	1.70	1.42	Pass
M-HW-4	1.3	1.66	0.61	0.45	1.36	1.19	1.62	1.67	1.40	Pass
						Average	**1.85**	**1.68**	-	Pass
C-HR-1	2.4	1.75	1.26	0.91	1.39	1.15	1.60	1.68	1.41	Pass
C-HR-2R	2.1	>1.39	0.77	0.52	1.47	1.15	1.69	1.64	1.38	Pass
C-HR-3	2.4	2.31	1.15	0.92	1.25	1.17	1.46	1.71	1.42	Pass
C-HR-4R	2.7	>1.49	1.06	0.59	1.80	1.17	2.11	1.65	1.39	Pass
						Average	**1.76**	**1.71**	-	Pass

5. Discussion

The introduction of the rafter proportioning limits, $h/b_f \leq 6$ and $A_w/A_f \leq 2.5$, was shown to be successful in developing stable post-peak response in the C-HR-2 and C-HR-4 frames. The path to this finding included additional supplementary work that sheds useful insight on the performance of these systems. Previously, it was found that purlin (bracing) stiffness was important to stable frame response; however, it was found here that once the purlin met the AISC 360 Appendix 6 bracing requirements, additional bracing stiffness did little to improve the post-peak response. Even an infinitely stiff purlin brace in a model of C-HR-4, therefore fully limiting LTB response to between the brace points, did not improve the post-peak ductility appreciably – as web bending and the LDB mode occurred in this condition. Thus, bracing stiffness alone, cannot improve the post-peak response of frames with rafters not meeting the proportioning limits.

The rafters in C-HR-2 and C-HR-4 meet strength requirements, but the post-peak failure mechanisms do not provide sufficient ductility (nor is enough overstrength present to account for a non-ductile response). The C-HR-2 and C-HR-4 rafter geometries are not typical – no steel rolled sections have the h/b_f or A_w/A_f of these shapes; only plate girders may have these dimensions. In the extensive study of moment-shear interaction in plate girders, White et al. (2008) studied 148 tests and only 14 had $h/b_f > 6$ and $A_w/A_f > 2.5$. They concluded that "the strength behavior of these types of members is dramatically different than that of the member types [that meet the proportioning limits]." This would ultimately be realized in the AISC 360 shear provisions where the limits are utilized to determine if the girder is stable enough to develop shear post-buckling and significant tension-field action; and is also the reason moment-shear interaction need not currently be checked in AISC 360.

Across the following reports and papers (Meimand et al., 2018; Moen et al., 2019; Nikoukalam et al., 2025), and including this study, a significant number of FEMA P-695 analyses have been conducted on metal building system frames. The results of all evaluations are provided in Table 7 and cover (i) clear span and modular metal building systems with, (ii) eave heights between 25 ft

[7.6 m] and 45 ft [13.7 m], and (iii) span lengths between 50 ft [15.2 m] and 200 ft [61.0 m], and (iv) walls with tributary weights up to 116 psf [5550 Pa], and (v) roofs loaded up to 30 psf [1440 Pa]. ASCE 7-16 OMF designs use a seismic response modification coefficient, R, to account for overstrength and ductility of 3.0. It is observed that this R is supported by a typical metal building frame overstrength of 2.0 and ductility of 2.0. All criteria of AISC 360 must be adhered to in an OMF design – and previous work shows the particular importance of meeting the Appendix 6 bracing provisions. New from this paper is the additional limitation that rafter geometric proportioning limits, consistent with the AISC 360 shear provisions for TFA, are also necessary. Taken together, the simulations provide a strong underpinning for the codified seismic design of metal building system frames in the United States.

Table 7. Summary table of all archetype buildings studied during 2018-2025

Reference	Archetype	Frame	Wall Weight [2]	Roof Load [3]	N × Span	Eave Height	Overstrength	Period-Based Ductility	h/b_f [1]	A_w/A_f [1]	Drift Limit	*ACMR*	$ACMR_{10\%}$	$ACMR_{20\%}$	Check (Pass/Fail)
					N × ft [m]	ft [m]	Ω_o	μ_T			%				
(Moen et al., 2019)	A1	Clear span	Heavy	Light	1 × 70 [21.3]	25 [7.6]	2.1	3.0	4.7	2.4	4.5	1.72	1.89	1.52	Pass
	A2	Clear span	Heavy	Light	1 × 70 [21.3]	45 [13.7]	1.1	4.2	5.7	4.3	4.5	2.50	2.15	1.52	Pass
	A3	Clear span	Light	Light	1 × 70 [21.3]	25 [7.6]	1.9	1.4	3.1	1.9	4.5	1.64	1.67	1.4	Pass
	A4	Clear span	Light	Light	1 × 200 [61.0]	35 [10.7]	3.3	1.7	4.2	1.3	4.5	1.72	1.64	1.38	Pass
(Nikoukalam et al., 2025)	AM1	Modular	Light	Light	2 × 50 [15.2]	25 [7.6]	2.3	1.9	3.5	1.5	6.0	1.54	1.7	1.42	Pass
	AM2	Modular	Light	Light	3 × 50 [15.2]	25 [7.6]	2.0	1.6	3.7	2.8	6.0	1.52	1.66	1.39	Pass
	AM3R	Modular	Light	Light	2 × 50 [15.2]	45 [13.7]	1.9	1.5	4.4	1.7	6.0	2.07	1.65	1.39	Pass
	AM4R	Modular	Light	Light	3 × 50 [15.2]	45 [13.7]	1.7	2.0	4.9	1.8	6.0	2.20	1.72	1.43	Pass
	AM5	Modular	Light	Light	2 × 100 [30.5]	25 [7.6]	2.3	1.5	4.8	1.8	6.0	1.48	1.65	1.39	Pass
	AM7	Modular	Light	Light	2 × 100 [30.5]	45 [13.7]	2.0	1.6	4.9	2.4	6.0	1.69	1.67	1.4	Pass
This study	M-HW-1	Modular	Heavy	Light	2 × 50 [15.2]	45 [13.7]	1.7	1.9	3.9	1.3	4.5	2.09	1.7	1.42	Pass
	M-HW-2	Modular	Heavy	Light	2 × 100 [30.5]	45 [13.7]	1.8	1.5	4.9	2.5	4.5	1.73	1.65	1.39	Pass
	M-HW-3	Modular	Heavy	Heavy	2 × 50 [15.2]	45 [13.7]	1.7	1.9	4.7	1.9	4.5	1.94	1.7	1.42	Pass
	M-HW-4	Modular	Heavy	Heavy	2 × 100 [30.5]	45 [13.7]	1.3	1.7	4.8	2.4	4.5	1.62	1.67	1.4	Pass
	C-HR-1	Clear span	Light	Heavy	1 × 50 [15.2]	25 [7.6]	2.4	1.8	4.9	2.2	4.5	1.60	1.68	1.41	Pass
	C-HR-2R	Clear span	Light	Heavy	1 × 50 [15.2]	45 [13.7]	2.1	1.8	5.2	1.4	4.5	1.69	1.64	1.38	Pass
	C-HR-3	Clear span	Light	Heavy	1 × 100 [30.5]	25 [7.6]	2.4	2.3	4.4	2.2	4.5	1.46	1.71	1.42	Pass
	C-HR-4R	Clear span	Light	Heavy	1 × 100 [30.5]	45 [13.7]	2.7	1.8	4.9	1.2	4.5	2.11	1.65	1.39	Pass
						Average	**2.0**	**1.9**	-	-	-	**1.80**	**1.71**	-	Pass

[1] Rafter proportions are provided in the second braced span from the knee.
[2] Heavy wall and light wall self-wight is defined as 75-116 psf [3590-5550 Pa] and ~2 psf [96 Pa], respectively.
[3] Heavy roof and light roof dead load is defined as 30 psf [1440 Pa] and 15-20 psf [718-958 Pa], respectively.
h: rafter web depth
b_f: rafter flange width
A_w: area of the rafter web
A_f: area of the rafter flange

6. Summary and Conclusion

This study evaluated the seismic performance of modular and clear span metal building systems with heavier wall and roof loads in high seismic zones, using the FEMA P-695 methodology. The motivation for this investigation stems from the ongoing effort to assess whether the current seismic design parameters assigned to Ordinary Moment Frames (OMFs) remain valid when applied to metal building system frames beyond the post-Northridge limits on height and mass. While a previous study (Nikoukalam et al., 2025) confirmed the adequacy of OMF seismic parameters for typical modular systems with light wall (2 psf [96 Pa]) and roof loads (<20 psf [958 Pa]), the present study specifically targeted configurations with heavier wall (116 psf [5550 Pa]) and roof (30 psf [1440 Pa]) to determine whether additional limits or design considerations are needed.

Eight archetypes were developed in collaboration with industry, covering two performance groups: modular buildings with precast concrete wall panels (M-HW) and clear span buildings with heavier-than-typical roof loading (C-HR). High-fidelity shell finite element models were used to perform nonlinear static pushover and quasi-static cyclic analyses. Each archetype was also represented by a calibrated nonlinear SDOF model for efficient collapse assessment per FEMA P-695. A collapse drift limit of 4.5% was adopted for all archetypes, based on observed nonlinear behavior and consistency with prior studies (Moen et al., 2019).

All archetypes demonstrated adequate seismic performance and met the individual and group acceptance criteria of FEMA P-695. The modular heavy wall buildings generally exhibited stable post-peak behavior governed by rafter yielding, local buckling, and panel zone yielding. In the heavy roof clear span buildings, lateral-distortional buckling of rafter was identified as a critical limit state in taller buildings (45 ft. [13.7 m]). However, through section redesign incorporating proportioning limits inspired by AISC tension field action criteria, the redesigned systems exhibited improved stability and ductility.

The results support the use of OMF seismic design parameters (R = 3.5, Ω_o = 3, C_d = 3) for single-story metal building systems with roof dead loads up to 30 psf [1440 Pa] and building heights up to 45 ft [13.7 m], when supported by appropriate member proportioning and bracing practices. The findings also indicate that heavier exterior wall systems can be accommodated without compromising seismic performance. Overall, this study provides a basis for refining height and load-related design limits for OMFs in metal buildings and demonstrates that with proper detailing and proportioning, systems with increased mass demands can reliably meet seismic performance expectations.

7. Acknowledgments

The authors would like to thank the Metal Building Manufacturers Association (MBMA) Seismic Research Steering Group who provided thoughtful advice, input, effort, and feedback throughout this project. In addition, several engineers in this group, led by Mr. Igor Marinovic of BlueScope Buildings, NA, provided the complete designs for the metal building system archetypes. The authors would also like to thank the peer review panel comprised of Dr. Greg Deierlein, Dr. Michael Engelhardt, and Dr. Tom Sabol who reviewed the modeling protocols and conclusions in detail for the clear span seismic study that preceded this work. In addition, Dr. Chia-Ming Uang was gracious with his time and data during the validation phase of the modeling. Finally, Dr. Lee Shoemaker and Mr. Vincent Sagan of MBMA were instrumental in shepherding this project to a meaningful end. The team would also like to recognize the financial support of

MBMA in conducting the work.

8. References

AISC. (2010). ANSI/AISC 341-10, Seismic Provisions for Structural Steel Buildings. American Institute of Steel Construction.

AISC. (2016). Specification for Structural Steel Buildings AISC 360-16. American Institute of Steel Construction.

ASCE. (1998). Minimum Design Loads for Buildings and Other Structures. American Society of Civil Engineers.

ASCE. (2002). Minimum Design Loads for Buildings and Other Structures. American Society of Civil Engineers.

ASCE. (2016). Minimum Design Loads for Buildings and Other Structures. American Society of Civil Engineers.

ASCE. (2022). Minimum Design Loads and Associated Criteria for Buildings and Other Structures. In ASCE - Standards. American Society of Civil Engineers (ASCE). https://doi.org/10.1061/97870784415788

ATC. (2009). Quantification of Building Seismic Performance Factors (Issue FEMA-P695).

Kim, Y. D. (2010). Behavior and Design of Metal Building Frames with General Prismatic and Web-Tapered Steel I-Section Members. School of Civil and Environmental Engineering, Georgia Institute of Technology.

MathWorks. (2018). MATLAB Version 9.4 (R2018a). https://www.mathworks.com

McKenna, F., Fenves, G. L., & Scott, M. H. (2004). Open System for Earthquake Engineering Simulation.

Meimand, V., Moen, C., & Schafer, B. (2018). Examination of Seismic Response Modification Coefficients for Metal Building Systems with FEMA P695 Process. Proceedings of the 11th National Conference in Earthquake Engineering.

Moen, C. D., Torabian, S., & Schafer, B. W. (2019). Evaluation of Metal Building System Seismic Response Modification Coefficients. https://jscholarship.library.jhu.edu/items/3fb18f3a-c7e9-4696-b32a-188fd336af76

Nikoukalam, M. T., Torabian, S., & Schafer, B. W. (2025). Evaluation of Seismic Design Parameters for Modular Metal Buildings in High Seismic Zones. https://doi.org/https://doi.org/10.31224/4586

Prawel, S. P., Morrell, M. L., & Lee, G. C. (1974). Bending and buckling strength of tapered structural members. Welding Research Supplement, 53(February), 75–84.

Schafer, B. W., Li, Z., & Moen, C. D. (2010). Computational modeling of cold-formed steel. Thin-Walled Structures, 48(10–11), 752–762.

Simulia. (2014). ABAQUS Version 6.14.

Smith, M. D. (2013). Seismic testing and analytical studies for the development of new

seismic force resisting systems for metal buildings. Ph.D Dissertation, University of California, San Diego.

Smith, M. D., Turner, K. T., & Uang, C. M. (2013). Experimental Investigation of Cyclic Lateral Buckling of Web-Tapered I-Beams. Report No. SSRP-12.

Uang, C. M., Smith, M. D., & Shoemaker, W. L. (2011). Earthquake simulator testing of metal building systems. Structures Congress 2011, 693–704.

White, D. W., Michael, G. B., & Azizinamini, A. (2008). Shear Strength and Moment-Shear Interaction in Transversely Stiffened Steel I-Girders. Journal of Structural Engineering, 134(9), 1437–1449. https://doi.org/10.1061/(ASCE)0733-9445(2008)134:9(1437)

9. Appendix

Table A. Pinching 04 model parameters for all archetypes

		Archetype							
Parameter	**Unit**	**M-HW-1**	**M-HW-2**	**M-HW-3**	**M-HW-4**	**C-HR-1**	**C-HR-2R**	**C-HR-3**	**C-HR-4R**
ePf1	(kips)	89.3	104.7	82.8	88.8	22.4	20.2	41.4	46.8
ePd1	(in)	6.2	7.1	5.9	6.4	2.5	7.4	2.4	6.8
ePf2	(kips)	178.7	209.4	165.6	177.6	44.8	40.4	82.8	93.6
ePd2	(in)	13.2	14.4	12.1	12.8	5.1	14.8	4.9	13.7
ePf3	(kips)	223.4	261.8	207.0	222.0	56.0	50.5	103.5	117.0
ePd3	(in)	20.8	21.3	15.8	16.1	6.8	24.6	6.1	17.4
ePf4	(kips)	202.0	224.5	141.0	200.0	37.0	30.0	72.2	70.0
ePd4	(in)	31.5	32.0	31.5	32.0	14.7	42.0	14.6	32.4
eNf1	(kips)	-88.8	-103.6	-83.8	-88.8	-24.6	-20.1	-47.5	-45.2
eNd1	(in)	-6.1	-7.0	-5.9	-6.2	-2.8	-7.3	-2.8	-6.6
eNf2	(kips)	-177.6	-207.2	-167.6	-177.6	-49.1	-40.1	-95.0	-90.4
eNd2	(in)	-12.8	-14.1	-12.2	-12.7	-5.6	-14.7	-5.0	-13.2
eNf3	(kips)	-222.1	-259.0	-209.5	-222.0	-61.4	-50.1	-118.8	-113.0
eNd3	(in)	-21.0	-20.7	-15.8	-15.9	-6.4	-25.0	-5.7	-17.4
eNf4	(kips)	-202.5	-220.6	-146.0	-200.0	-35.9	-28.0	-69.9	-70.0
eNd4	(in)	-31.6	-32.1	-32.0	-32.0	-14.7	-42.0	-14.3	-32.4
rDispP	(-)	0.463	0.492	0.407	0.538	0.498	0.735	0.477	0.617
rForceP	(-)	0.988	0.797	0.715	0.700	0.718	0.888	0.747	0.825
uForceP	(-)	0.082	-0.330	-0.333	-0.332	-0.345	-0.097	-0.342	-0.293
rDispN	(-)	0.463	0.492	0.407	0.538	0.498	0.735	0.477	0.617
rForceN	(-)	0.988	0.797	0.715	0.700	0.718	0.888	0.747	0.825
uForceN	(-)	0.082	-0.330	-0.333	-0.332	-0.345	-0.097	-0.342	-0.293
gK1	(-)	-0.000124	0.0004701	0.0003455	2.41E-05	-0.000695	7.75E-05	-5.90E-04	7.73E-05
gK2	(-)	-0.000124	0.0004701	0.0003455	2.41E-05	-0.000695	7.75E-05	-5.90E-04	7.73E-05
gK3	(-)	-0.000124	0.0004701	0.0003455	2.41E-05	-0.000695	7.75E-05	-5.90E-04	7.73E-05
gK4	(-)	-0.000124	0.0004701	0.0003455	2.41E-05	-0.000695	7.75E-05	-5.90E-04	7.73E-05
gKLim	(-)	-0.000124	0.0004701	0.0003455	2.41E-05	-0.000695	7.75E-05	-5.90E-04	7.73E-05
gD1	(-)	-8.86E-05	0.0005727	1.86E-05	-0.0004713	-0.0001199	-1.84E-05	-4.84E-05	7.24E-05
gD2	(-)	-8.86E-05	0.0005727	1.86E-05	-0.0004713	-0.0001199	-1.84E-05	-4.84E-05	7.24E-05
gD3	(-)	-8.86E-05	0.0005727	1.86E-05	-0.0004713	-0.0001199	-1.84E-05	-4.84E-05	7.24E-05
gD4	(-)	-8.86E-05	0.0005727	1.86E-05	-0.0004713	-0.0001199	-1.84E-05	-4.84E-05	7.24E-05
gDLim	(-)	-8.86E-05	0.0005727	1.86E-05	-0.0004713	-0.0001199	-1.84E-05	-4.84E-05	7.24E-05
gF1	(-)	4.51E-05	-0.0005971	0.0002777	0.000522	0.0002581	2.17E-05	2.01E-04	6.78E-05
gF2	(-)	4.51E-05	-0.0005971	0.0002777	0.000522	0.0002581	2.17E-05	2.01E-04	6.78E-05
gF3	(-)	4.51E-05	-0.0005971	0.0002777	0.000522	0.0002581	2.17E-05	2.01E-04	6.78E-05
gF4	(-)	4.51E-05	-0.0005971	0.0002777	0.000522	0.0002581	2.17E-05	2.01E-04	6.78E-05
gFLim	(-)	4.51E-05	-0.0005971	0.0002777	0.000522	0.0002581	2.17E-05	2.01E-04	6.78E-05
gE	(-)	0.50	0.48	0.48	0.52	0.50	0.49	0.48	0.50
dmgType	(-)	'energy'	'energy'	'energy'	'energy'	'energy'	'energy'	'energy'	'energy'